

Exploring the Structure and Activity of Haloalkane Dehalogenase from *Sphingomonas paucimobilis* UT26: Evidence for Product- and Water-Mediated Inhibition^{†,‡}

Aaron J. Oakley,[§] Zbyněk Prokop,^{||} Michal Boháč,^{||} Jan Kmuníček,^{||} Tomáš Jedlička,^{||} Marta Monincová,^{||} Ivana Kutá-Smatanová,^{||,⊥} Yuji Nagata,[@] Jíří Damborský,^{*,||} and Matthew C. J. Wilce^{*,§}

Department of Pharmacology/Crystallography Centre, University of Western Australia, 35 Stirling Highway, Crawley, WA 6009, Australia, National Centre for Biomolecular Research, Masaryk University, Kotlarska 2, 611 37 Brno, Czech Republic, and Graduate School of Life Sciences, Tohoku University, Katahira, Sendai 980-8577, Japan

Received August 30, 2001; Revised Manuscript Received January 23, 2002

ABSTRACT: The hydrolysis of haloalkanes to their corresponding alcohols and inorganic halides is catalyzed by α/β -hydrolases called haloalkane dehalogenases. The study of haloalkane dehalogenases is vital for the development of these enzymes if they are to be utilized for bioremediation of organohalide-contaminated industrial waste. We report the kinetic and structural analysis of the haloalkane dehalogenase from *Sphingomonas paucimobilis* UT26 (LinB) in complex with each of 1,2-dichloroethane and 1,2-dichloropropane and the reaction product of 1-chlorobutane turnover. Activity studies showed very weak but detectable activity of LinB with 1,2-dichloroethane [$0.012 \text{ nmol s}^{-1} (\text{mg of enzyme})^{-1}$] and 1,2-dichloropropane [$0.027 \text{ nmol s}^{-1} (\text{mg of enzyme})^{-1}$]. These activities are much weaker compared, for example, to the activity of LinB with 1-chlorobutane [$68.2 \text{ nmol s}^{-1} (\text{mg of enzyme})^{-1}$]. Inhibition analysis reveals that both 1,2-dichloroethane and 1,2-dichloropropane act as simple competitive inhibitors of the substrate 1-chlorobutane and that 1,2-dichloroethane binds to LinB with lower affinity than 1,2-dichloropropane. Docking calculations on the enzyme in the absence of active site water molecules and halide ions confirm that these compounds could bind productively. However, when these moieties were included in the calculations, they bound in a manner similar to that observed in the crystal structure. These data provide an explanation for the low activity of LinB with small, chlorinated alkanes and show the importance of active site water molecules and reaction products in molecular docking.

Due to environmental problems arising from the production and use of halogenated hydrocarbons, the study of microbial enzymes that can catabolize these compounds is of major interest (1). Haloalkane dehalogenases (EC 3.8.1.5) make up one such important class of enzyme because of their ability to attack polychlorinated aliphatic hydrocarbons, which are produced in several industrial processes (2, 3). Haloalkane dehalogenases remove halides from organic compounds via a hydrolytic mechanism that results in the production of the corresponding alcohol, inorganic halide,

and hydrogen ion. One such haloalkane dehalogenase, LinB,¹ is isolated from a γ -hexachlorocyclohexane degrading bacterial strain *Sphingomonas paucimobilis* UT26 (4). It is the second enzyme in the biochemical pathway enabling the bacterium to utilize γ -hexachlorocyclohexane as its sole carbon and energy source (5).

LinB is a haloalkane dehalogenase of the α/β hydrolase family, with a main domain consisting of an eight-stranded β -sheet flanked with α -helices, and a cap domain which is comprised of α -helices and several loops (6, 7). The active site is formed by the close interactions of the two domains (Figure 1). Catalysis by this family of dehalogenases is thought to take place in two steps (8). Once substrate binds with the scissile halide in the binding site formed by Trp109, Asn38, and Pro208, the carboxylate group of Asp108 makes a nucleophilic attack upon the scissile carbon. Inorganic halide is released with the concomitant formation of an ester intermediate formed by the alkane and Asp108. A nearby water molecule undergoes deprotonation by His272 and attacks the ester linkage, resulting in the formation of the

[†] Financial support from the Australian Research Council (Grant A00001093) and the Czech Ministry of Education (Grant LN00A016) is acknowledged. A.J.O. is the recipient of an Australian Research Council Postdoctoral Research Fellowship. M.C.J.W. is supported by the Raine Foundation. M.B. acknowledges the MCB 2000 Studentships from the University of Western Australia.

[‡] Coordinate and X-ray amplitudes have been deposited at the Research Collaboratory for Structural Bioinformatics Protein Data Bank: PDB entry 1G5F for the complex with 1,2-dichloroethane, PDB entry 1G42 for the complex with 1,2-dichloropropane, and PDB entry 1G4H for the complex with butan-1-ol.

* To whom correspondence should be addressed. J.D.: fax, +420-5-41129506; e-mail, jiri@chemi.muni.cz. M.C.J.W.: fax, +618-9346-3469; e-mail, mwilce@receptor.pharm.uwa.edu.au.

[§] University of Western Australia.

^{||} Masaryk University.

[⊥] Present address: Photosynthesis Research Center, South Bohemian University, Branišovská 31, 370 05 České Budějovice, Czech Republic.

[@] Tohoku University.

¹ Abbreviations: DhIA, haloalkane dehalogenase from *Xanthobacter autotrophicus* GJ10; DhaA, haloalkane dehalogenase from *Rhodococcus erythropolis* strains Y2, m15-3, HA1, GJ70, NCIMB13064, and TB2; LinB, haloalkane dehalogenase from *Sphingomonas paucimobilis* UT26; rmsd, root-mean-square deviation; 1,2-DCP, 1,2-dichloropropane; 1,2-DCE, 1,2-dichloroethane; 1-CB, 1-chlorobutane.

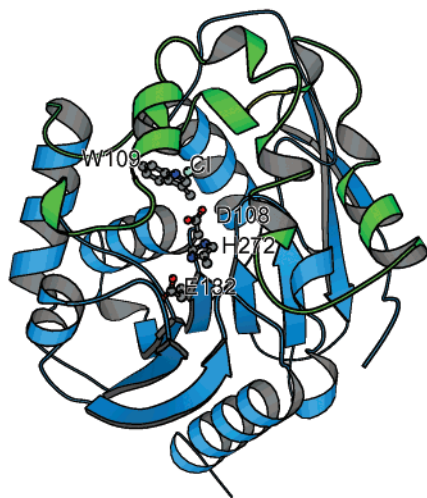


FIGURE 1: LinB structure in Richardson representation. The core (main) domain is colored blue. The cap domain is colored green. The active site residues (Asp108, Trp109, Glu132, and His272) are shown in ball-and-stick representation. The halide binding site is indicated by the Cl^- ion.

alcohol product and free Asp108. Site-directed mutagenesis of LinB confirms that Asp108, His272, and Glu132 comprise the catalytic triad in that enzyme (9).

The broad substrate specificity of LinB could make it useful in bioremediation; however, LinB is inhibited by the key pollutants 1,2-dichloroethane (1,2-DCE) and 1,2-dichloropropane (1,2-DCP). These compounds are economically important; ~ 7230000 tons of 1,2-DCE was produced in the United States in 1992 by various industrial processes (10). 1,2-DCP is formed as a byproduct in the synthesis of propylene oxide and epichlorohydrin (11), and is a problematic pollutant because it is not catalyzed efficiently by any of the haloalkane dehalogenases. 1,2-DCP is recalcitrant under aerobic conditions (11, 12). We have investigated the structural and kinetic aspects of LinB with 1,2-DCE and 1,2-DCP to determine the reasons for the low activity of LinB with these compounds. For comparison, we have also attempted to determine the structure of LinB in complex with the model substrate 1-chlorobutane (1-CB). This information is crucial in the effort to design an enzyme with improved catalytic properties for these compounds.

MATERIALS AND METHODS

Crystallization. LinB was cloned, overexpressed, purified, and crystallized as described previously (13). Briefly, crystals of LinB grew as plates with dimensions of 0.8 mm \times 0.4 mm \times 0.2 mm using the hanging drop vapor diffusion method. The mother liquor contained 18% PEG 6000, 0.2 M calcium acetate, and 0.1 M Tris (pH 8.9).

Soaking Experiments. Crystals of LinB were transferred using a cryoloop (Hampton Research) from the mother liquor to a 2 μL hanging drop of cryoprotectant [0.1 M tris-(hydroxymethyl)aminomethane buffer (pH 8.9), 0.2 M calcium acetate, 18% polyethylene glycol 6000, and 20% (v/v) glycerol] on a siliconized cover slip. The compound of interest (10 μL) was placed into a well containing 1 mL of cryoprotectant solution. The halogenated compounds then entered the crystal via vapor diffusion from the reservoir. The cover slip was sealed on top using vaseline. The soak times and temperature were chosen according to the enzy-

Table 1: Soaking and Data Collection Statistics for the LinB–Ligand Complex

	1,2-DCE	1,2-DCP	1-CB
Data Collection			
soak time (min)	60	30	60
soak temperature ($^{\circ}\text{C}$)	20	20	4
space group	$P2_12_12$	$P2_12_12$	$P2_12_12$
cell dimensions			
a (\AA)	50.9	50.8	50.8
b (\AA)	71.9	72.0	72.0
c (\AA)	73.3	73.3	73.3
maximum resolution (\AA)	1.8	1.8	1.8
no. of crystals	1	1	1
total no. of observations	54733	55091	57835
no. of unique reflections	23846	24918	24212
completeness of data (%) ^a	93.2 (91.0)	97.0 (95.7)	94.3 (95.9)
data $> 3\sigma_1$ (%)	65.8 (12.5)	77.0 (41.3)	75.3 (50.5)
I/σ_1	10.8 (2.1)	12.8 (3.0)	19.6 (3.5)
multiplicity	2.3 (2.2)	2.2 (2.1)	2.4 (2.3)
R_{merge} (%) ^b	7.2 (35.9)	5.4 (24.1)	4.0 (34.5)
Refinement Statistics			
no. of non-hydrogen atoms	2673	2795	2611
no. of protein atoms	2356	2346	2357
no. of ligand atoms	8	15	15
no. of solvent molecules	291	422	237
no. of ions	4	2	3
R_{factor} (%) ^c	17.5 (27.3)	16.4 (22.4)	18.5 (28.0)
R_{free} (%) ^d	20.4 (30.1)	19.8 (25.7)	20.5 (27.9)
rmsd from ideal geometry			
bonds (\AA)	0.005	0.005	0.005
angles (deg)	1.3	1.3	1.3
dihedrals (deg)	22.5	22.4	22.5
impropers (deg)	0.85	0.85	0.84
bonded B^2 's (\AA^2)	1.457	1.15	0.50
residues in most favorable region of a Ramachandran plot	87.4	86.6	85.8

^a Numbers in parentheses refer to the highest-resolution bin (1.9–1.8 \AA). ^b $R_{\text{merge}} = \sum_i \sum_l |I_{hi} - \langle I_{hl} \rangle| / \sum_i \sum_l I_{hl}$. ^c $R_{\text{factor}} = \sum_h ||F_{\text{obs}}| - |F_{\text{calc}}|| / \sum_h |F_{\text{obs}}|$ where F_{obs} and F_{calc} are the observed and calculated structure factors, respectively. ^d R_{free} was calculated based on 5% of the diffraction data not used in the refinement.

matic activity of LinB toward the compound of interest. Information for each soak is shown in Table 1.

X-ray Data Collection and Processing. Protein crystals were mounted with cryoprotectant in a loop (Hampton Research) and kept frozen using an Oxford Cryostream Cooler (Oxford Cryosystems). Data were collected using a MAR345 area detector (Mar Research) using $\text{Cu K}\alpha$ X-rays ($\lambda = 1.5418 \text{\AA}$) from a Rigaku RU-200 rotating anode generator. X-rays were focused using nickel-coated gold mirrors (Mar Research). Consecutive batches of 0.25° oscillations were collected. Data were processed using the HKL package (14).

Structure Solution and Refinement. Structures were determined using the wild-type LinB structure (PDB entry 1CV2) with all nonprotein atoms removed. At all stages during refinement, R_{free} validation based on randomly selected reflections (5% of the total set) was used. The structures were refined as follows. Molecular replacement models were subjected to rigid body, positional, and B -factor refinement in CNS (15), followed by 20 cycles of automatic refinement by CCP4/ARP (16) that included the automatic building of water molecules. Water molecules that were built into the active site and halide binding site were omitted from the models, and further positional and B -factor refinement was conducted to reduce phase bias. Sigma-A weighted electron

density maps were generated from these models and inspected using O (17).

Some large spherical peaks in the solvent were interpreted as Ca^{2+} ions (a component of the crystallization mixture), as they appeared to be coordinated by water molecules. These were built into the density and included in later rounds of refinement. Ligand models were built into electron density after extensive inspection of $2F_o - F_c$ and $F_o - F_c$ maps. The locations of chlorine atoms of the compounds were identified by their increased peak heights in the $F_o - F_c$ maps. Bond and angle parameters for the ligands were derived using XPLO2D (18) from models produced with WebLab Viewer Pro 3.5 (Molecular Simulations Inc.). For all ligands, there was more electron density than the binding of the ligand in one orientation could account for, and hence, multiple models for the ligand were inserted. Special care was taken in the modeling of these ligands because of overlap.

Structure Analysis. Intermolecular contacts between the ligand and protein were assessed using CONTACT (19). Model quality was assessed using CNS (15) and MOLEMAN (20). The quality of the structures was analyzed using PROCHECK (19) and MOLEMAN (20). LSQMAN (21) was used to superimpose models for comparison.

Activity Measurements. Enzymatic activity of LinB was assessed by determination of the substrate and product concentrations using gas chromatography–mass spectrometry (GC–MS). The reaction was conducted in 1.5 mL screw-cup vessels. The reaction was initiated by adding 200 μL of enzyme solution (0.4 mM) into 0.8 mL of substrate solution [0.57 mM 1,2-DCE and 0.51 mM 1,2-DCP, respectively, dissolved in a glycine buffer (pH 8.6)]. The mixture was incubated at 37 °C and analyzed every 20 min for 4 h for product formation. At each time point, 1 μL of the reaction mixture was analyzed by GC–MS (Trace MS 2000, Thermo Finnigan) equipped with an SSL Injector and DB5-MS 25 m \times 0.25 mm \times 0.25 μm capillary column (J&W Scientific). The reaction mixture without enzyme served as an abiotic control.

Inhibition Kinetics. Inhibition kinetics of LinB were studied by determination of the substrate and product concentrations using gas chromatography (Trace GC 2000, Thermo Finnigan) equipped with a flame ionization detector and the DB-FFAP 30 m \times 0.25 mm \times 0.25 μm capillary column (J&W Scientific). Dehalogenation reactions were performed in 25 mL Reacti-Flasks closed by Mininert valves in a shaking water bath at 37 °C. The reaction mixture (pH 8.6) consisted of the enzyme preparation and varied concentrations (0.05–6.5 mM) of the substrate 1-chlorobutane and varied concentrations (0–26 mM) of the inhibitor 1,2-DCE or 1,2-DCP. The reaction was stopped by the addition of ethanol. The data, measured in triplicate, were fitted to different inhibition models. The steady-state inhibition constants were calculated using the computer program EZ-Fit version 1.1.²

Molecular Docking. Substrate and product molecules were docked in the active sites using the program AUTODOCK 3.0 (22). Crystal water molecules retained in the enzyme active site in some of the dockings were treated as a part of

the rigid enzyme. Substrates and products were treated as flexible molecules. The WHATIF 5.0 program (23) was used for adding the polar hydrogen atoms on protein structures. His289 was singly protonated on N_δ in accordance with its catalytic function. Charges were added on all enzyme atoms using the script q.kollua. Solvation parameters were added to the atoms in the protein structure by the script addsol. The grid maps were calculated using AUTOGRID 3.0 with 81 \times 81 \times 81 points and grid spacing of 0.25 Å. The Lamarckian genetic algorithm (24) was used with a population of 50 individuals, a maximum number of generations of 27 000, an elitism value of 1, a mutation rate of 0.02, and a crossover rate of 0.50. The local search was based on the pseudo-Solis and Wets algorithm (25) with a maximum of 300 iterations per local search. Final orientations from every docking were clustered with the clustering tolerance for the root-mean-square positional deviation (0.5 Å). Fifty docking runs were performed for each enzyme–substrate complex.

RESULTS

1,2-DCE Complex Crystal Structure. Despite this compound being an inhibitor (4), strong density interpretable as a Cl^- ion was observed in the halide binding site. The distances between the Cl^- ion and Trp109 $\text{N}_{\epsilon 1}$, Asn38 $\text{N}_{\delta 2}$, and Pro208 N were 3.2, 3.5, and 3.5 Å, respectively. A large volume of electron density was seen in the active site of LinB, and was interpreted as 1,2-DCE bound in two orientations (Figure 2a). Both ligand models are oriented with one well-ordered chlorine atom binding in a pocket in the active site comprising residues Leu248, Ala247, Pro144, and Leu177. Each ligand was given an occupancy of 0.5. The other chlorine atoms are placed divergently between the two ligand models pointing toward the halide binding pocket. They appear less well ordered as their electron density is spread out more. A water molecule located close to these ligands was observed to be 2.6 Å away from the Asp147 $\text{O}_{\delta 2}$ atom, which was shifted 1.8 Å (measured from atom $\text{O}_{\delta 2}$) parallel to the ligand compared with the apoenzyme structure. No other shifts in the active site residues were observed. The inhibitor molecules contact residues Leu177, Asp108, and His272. The small number of contacts of the ligand with the protein would explain the relative disorder of this molecule. This ligand displaces three water molecules (observed in the free enzyme structure) from the active site.

1,2-DCP Complex Crystal Structure. The electron density in the active site was interpreted as 1,2-DCP bound in at least two conformations (Figure 3a). There was no evidence that the compound had been hydrolyzed and no evidence for the covalent modification of catalytic residue Asp108. The halide binding site contained an area of spherical density that was interpreted as a chloride ion. Since a racemic mixture was used, the two possible enantiomers were built into the active site in overlapping conformations. The refined model yielded excellent quality electron density with no peaks in $F_o - F_c$ maps. Attempts to remove one or more of the models and subject the model to further refinement gave peaks ($>3\sigma$) in the resulting $F_o - F_c$ maps. Each ligand model was given an occupancy of 0.5. None of the ligand models are bound productively. They are located adjacent to the face of the catalytic His272 residue (Figure 3a). The closest ligand Cl atom is 5.2 Å away from the chloride

² By F. W. Perrella.

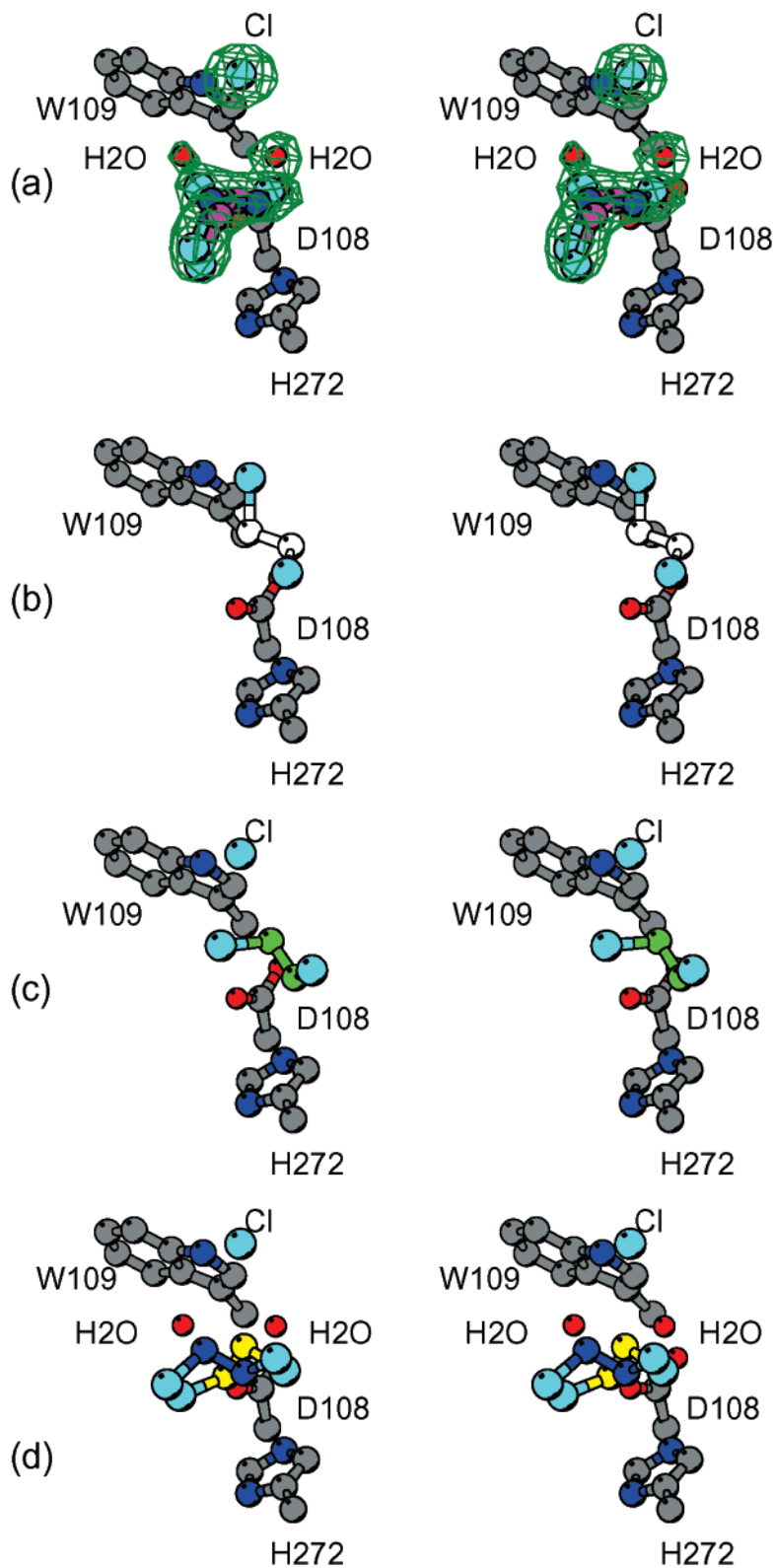


FIGURE 2: Stereodiagrams of experimentally determined and docked models of 1,2-DCE binding in the active site of LinB. Important catalytic residues are indicated in ball-and-stick representation. (a) Crystallographically determined binding of 1,2-DCE with surrounding water and Cl^- ion. A $2F_o - F_c$ electron density map contoured at 1σ shown for all ligands represented in green. The two ligands are represented with carbon atoms colored blue and magenta and Cl atoms in cyan. Panels b–d represent the different modeling experiments with various combinations of Cl^- and water molecules included in the calculations. The models are represented with carbon atoms colored as follows: (b) white for model 1, (c) green for model 2, and (d) yellow for model 3 and blue for model 4. The details of the modeling experiments are given in Table 3.

binding site and 5.0 \AA away from the Asp108 $\text{O}_{\delta 1}$ atom. A catalytic water molecule was observed 2.89 \AA from Asp108 $\text{O}_{\delta 1}$. The models contact residues Val173, Leu177, Phe169,

Asp108, and His272. Two differences were noted in the side chain configurations of the 1,2-DCP complex compared with the free enzyme structure. The side chain of Asp147 is

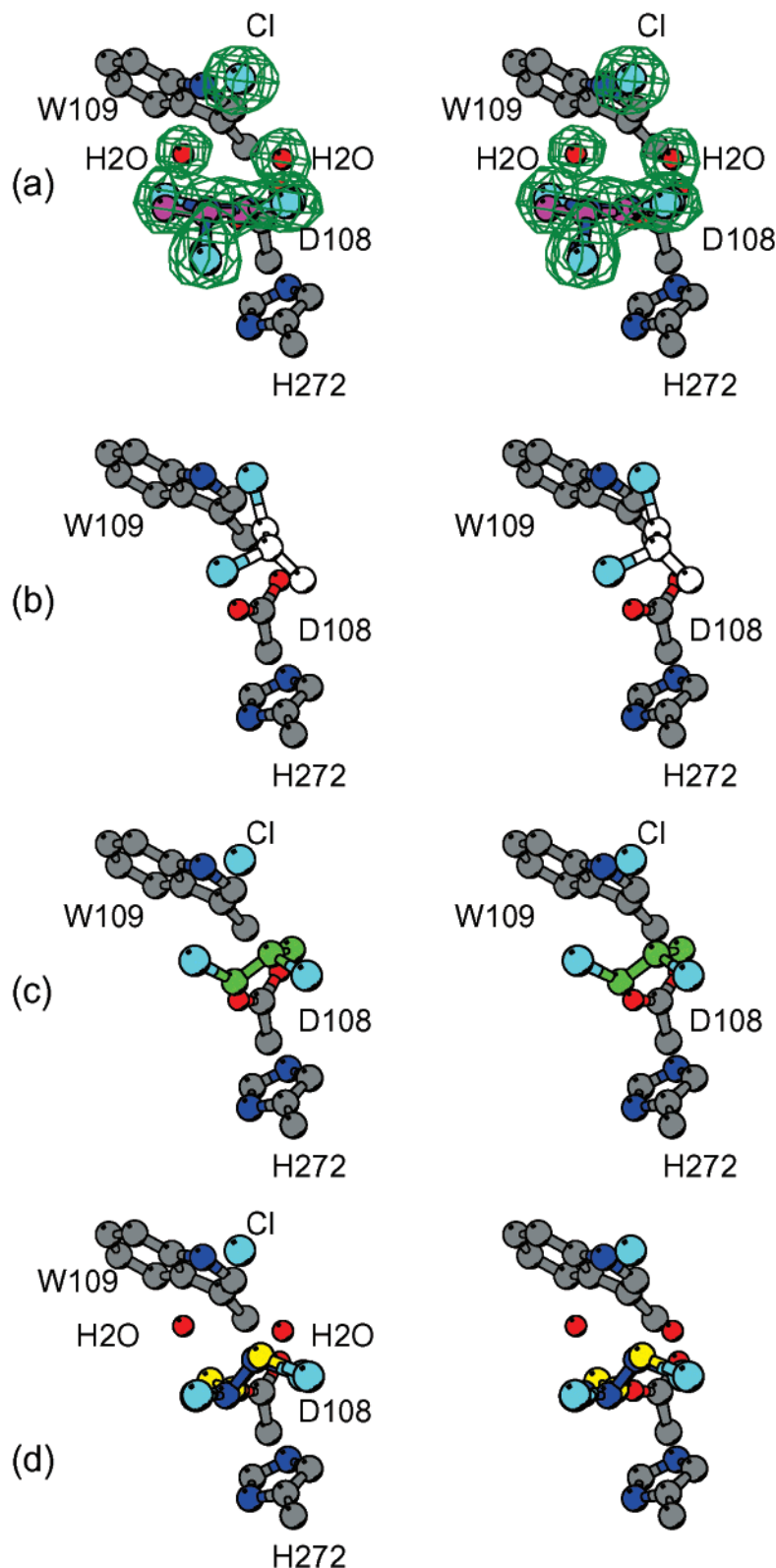


FIGURE 3: Stereodiagrams of experimentally determined and docked models of 1,2-DCP binding in the active site of LinB. Important catalytic residues are indicated in ball-and-stick representation. (a) Crystallographically determined binding of 1,2-DCP with surrounding water and Cl^- ion. A $2F_o - F_c$ electron density map contoured at 1σ shown for all ligands represented in green. The two ligands are represented with carbon atoms colored blue and magenta and Cl atoms in cyan. Panels b–d represent the different modeling experiments with various combinations of Cl^- and water molecules included in the calculations. The models are represented with carbon atoms colored as follows: (b) white for model 1, (c) green for model 2, and (d) yellow for model 3 and blue for model 4. The details of the modeling experiments are given in Table 3.

observed to lie in two conformations, one of which matches the free enzyme structure; the other has shifted parallel to the ligand such that it forms part of the tunnel to the active

site (the shift in the Asp147 $\text{O}_{\delta 2}$ atom was observed to be 1.9 Å). Phe143 has shifted (the shift in C_{ζ} was 1.3 Å) such that it is closer to the ligand. The ligands displace three water

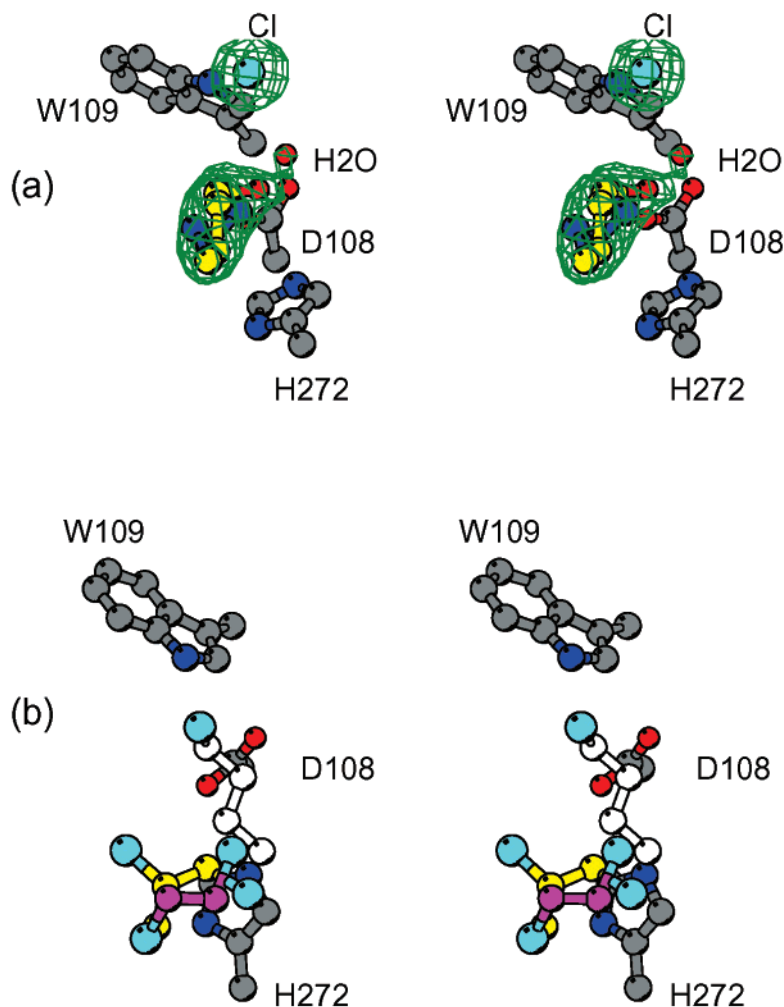


FIGURE 4: (a) Stereodiagram of the crystallographically determined binding location of 1-CB turnover product 1-butanol. A $2F_o - F_c$ electron density map contoured at 1σ shown for all ligands represented in green. The two conformers are shown with carbon atoms colored blue and yellow. Important catalytic residues are indicated in ball-and-stick representation. (b) Comparison of crystallographically determined 1,2-DCE and 1,2-DCP structures vs 1-CB docked in the active site as it would be found prior to S_N2 attack. Chlorine atoms are represented in cyan, with carbon atoms colored according to molecule: yellow for 1,2-DCP, magenta for 1,2-DCE, and white for 1-CB.

molecules found in the active site in the free enzyme structure.

1-Butanol Complex Crystal Structure. The compound has previously been observed to act as a substrate of LinB with an activity of $68.2 \text{ nmol s}^{-1} (\text{mg of enzyme})^{-1}$. Despite the compound being soaked at 4°C , the density in the active site indicated that the compound had been hydrolyzed. A single chloride ion was placed between Trp109, Asn38, and Pro208 (distances between Cl^- and the Trp109 $\text{N}_{\epsilon 1}$, Asn38 $\text{N}_{\delta 2}$, and Pro208 N atoms of 3.3, 3.6, and 3.4 Å, respectively). A 1-butanol molecule was modeled in the active site in two positions with each model given an occupancy of 0.5 (Figure 4a). The distances between the 1-butanol oxygen and Asp108 $\text{O}_{\delta 1}$ are 3.5 and 3.8 Å for each conformation. A water molecule 2.7 Å from Asp108 $\text{O}_{\delta 1}$ appears to have replaced the substrate water molecule forming the OH group of 1-butanol in the reaction. The only observed shift in the active site was the deflection of the Asp147 side chain toward the 1-butanol molecule (the distance between the positions of $\text{O}_{\delta 2}$ of the wild type and the complex structure is 2.1 Å). The distance between Asp147 $\text{O}_{\delta 1}$ and atom C_4 of the reaction product is 3.2 Å. The 1-butanol models contact residues Asp108, Pro144, Asp147, Ala247, and His272. The 1-butanol molecule displaces two water molecules in the free

enzyme active site. A 1-butanol molecule was also observed bound on the surface of the enzyme away from the active site, contacting residues Thr264, Phe289, and Arg292.

Structure Comparisons. The structures were compared with the free enzyme (PDB entry 1CV2) and the enzyme complexed with propane-1,3-diol (PDB entry 1D02). The 1,2-DCP, 1-butanol, and 1,2-DCE complexes superimpose on the free enzyme with rmsds of 0.50, 0.17, and 0.58 Å over all C_α atoms, respectively. The greatest divergences between the structures are at the N- and C-termini, which are relatively disordered in the structures. The active site residues superimpose closely in all cases. The greatest shifts are in the side chain position of Asp147 and Phe143 (described above). The ligands described here roughly superimpose, all being located adjacent to the His272 side chain; however, the propane-1,3-diol molecule described previously (6) is closer to the Asp108 carboxylate group. One of the OH groups of propane-1,3-diol is 3.1 Å away from Asp108 $\text{O}_{\delta 1}$, as opposed to 3.5 Å in the case of 1-butanol described above.

Dehalogenation of 1,2-DCE and 1,2-DCP by LinB. No detectable activity was observed in previous kinetic analyses of enzymatic dehalogenation of 1,2-DCE and 1,2-DCP by LinB (4). The presence of chloride ions in the active site of

Table 2: Kinetic Constants of the Haloalkane Dehalogenase LinB with the Substrate 1-Chlorobutane in the Presence of Inhibitors 1,2-Dichloroethane and 1,2-Dichloropropane

	K_m (mM)	K_i (mM)	k_{cat} (s^{-1})
1,2-DCE	0.25 ± 0.057	2.31 ± 0.550	1.05 ± 0.053
1,2-DCP	0.26 ± 0.002	0.97 ± 0.085	0.91 ± 0.027

LinB complexed with 1,2-DCE and 1,2-DCP (see above) suggested that these molecules may be converted by LinB, and thus, improvements to the experimental design were made to lower the detection limit of the activity assay. This measurement showed very weak but detectable activity of LinB with 1,2-DCE [$0.012 \text{ nmol s}^{-1} (\text{mg of enzyme})^{-1}$] and 1,2-DCP [$0.027 \text{ nmol s}^{-1} (\text{mg of enzyme})^{-1}$]. These activities are much weaker compared to the activity of LinB with 1-CB [$68.2 \text{ nmol s}^{-1} (\text{mg of enzyme})^{-1}$].

Inhibition of LinB by 1,2-DCE. The inhibition of 1-CB hydrolysis by 1,2-DCE was studied by steady-state kinetic analysis (Table 2 and Figure 5a). The identical slopes of the Hanes–Woolf plot suggest that the limiting initial velocity in the presence of 1,2-DCE was equal to the limiting initial velocity in its absence; however, the apparent K_M increased in the presence of 1,2-DCE. This suggests that, at any concentration of 1,2-DCE, a portion of the enzyme exists in the enzyme–inhibitor form which had no affinity for 1-CB. In addition, the initial velocity was driven to zero by increasing 1,2-DCE concentrations at a fixed substrate concentration (Figure 5c). The experimental data were analyzed by fitting the equations for competitive ($SE_{fit} = 0.0014$), uncompetitive ($SE_{fit} = 0.0025$), noncompetitive ($SE_{fit} = 0.0023$), and mixed noncompetitive ($SE_{fit} = 0.0039$) inhibition. The 1,2-DCE inhibition data fitted best to the competitive model with a K_i of $2.31 \pm 0.55 \text{ mM}$. LinB has 10 times lower affinity for 1,2-DCE than for 1-CB ($K_m = 0.25 \pm 0.057 \text{ mM}$; Table 2). The simple competitive inhibition of 1-CB hydrolysis by 1,2-DCE was deduced from these findings.

Inhibition of LinB by 1,2-DCP. An inhibition of 1-CB hydrolysis by 1,2-DCP was probed by steady-state kinetic analysis (Table 2). The Hanes–Woolf plot shows the effect of 1,2-DCP on the apparent K_M while the limiting initial velocity was equal in both the presence and absence of the inhibitor (Figure 5b). In addition, the initial velocity was driven to zero by increasing 1,2-DCP concentrations at a fixed substrate concentration (Figure 5c). The apparent K_M increased in the presence of 1,2-DCP, suggesting that at any concentration of 1,2-DCP, a portion of the enzyme existed in enzyme–inhibitor form with no affinity for 1-CB. The data were analyzed by fitting the equations for competitive ($SE_{fit} = 0.0007$), uncompetitive ($SE_{fit} = 0.0015$), noncompetitive ($SE_{fit} = 0.0016$), and mixed noncompetitive ($SE_{fit} = 0.0012$) inhibition. The 1,2-DCP inhibition data fitted best to the competitive model with a K_i of $0.97 \pm 0.085 \text{ mM}$ (Table 2). The simple competitive inhibition of 1-CB hydrolysis by 1,2-DCP was deduced from these findings.

Docking Calculations. Initially, the ligands were docked in the free protein molecule without any cofactors (water molecules and ions). These calculations did not reproduce crystallographically determined positions of the ligands in the active site. Ligand molecules were docked in positions

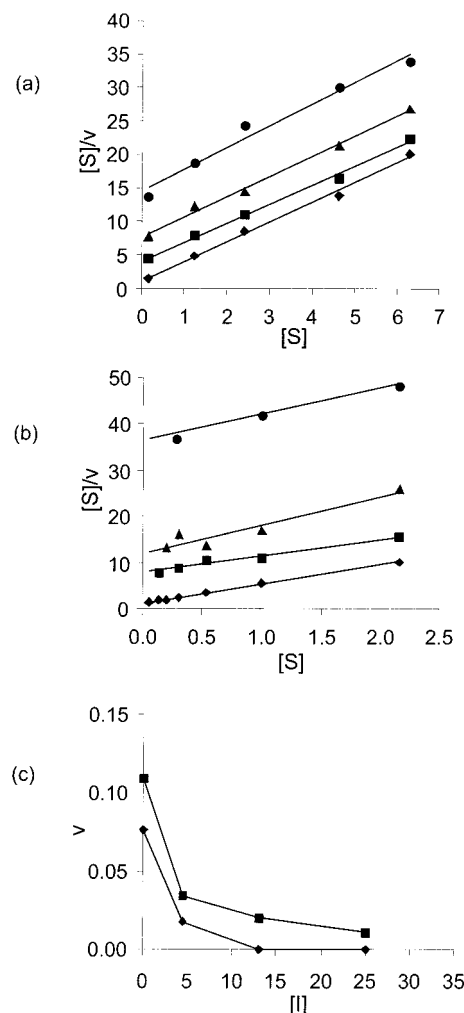


FIGURE 5: 1,2-DCE and 1,2-DCP inhibition kinetics. (a) Hanes–Woolf plot ($[S]$ vs $[S]/v$) demonstrating the effect of 1,2-DCE on the hydrolysis of 1-CB by LinB. The velocities (v) were determined in the presence of 0 (\blacklozenge), 5 (\blacksquare), 14 (\blacktriangle), and 26 mM 1,2-DCE (\bullet). (b) Hanes–Woolf plot ($[S]$ vs $[S]/v$) demonstrating the effect of 1,2-DCP on 1-CB hydrolysis. The velocities (v) were obtained in the presence of 0 (\blacklozenge), 4 (\blacksquare), 12 (\blacktriangle), and 22 mM 1,2-DCP (\bullet). (c) Plot of velocity of 1-CB hydrolysis (v) vs inhibitor concentration ($[I]$) at a substrate concentration of 0.15 mM for 1,2-DCE inhibition (\blacksquare) and 0.14 mM for 1,2-DCP inhibition (\blacklozenge).

suitable for a S_N2 dehalogenation reaction with a halogen atom in a position equivalent to the Cl^- ion and adjacent carbon atom oriented toward the nucleophile Asp108 (Figures 2 and 3, model 1). Detailed exploration of the enzyme–substrate and enzyme–product complexes revealed the possible importance of the active site waters and halide ion for binding of small ligands in the active site. We decided to study the effects of the presence and absence of halogen anion in the enzyme active site and the presence and absence of active site water molecules on ligand orientations. The result of the docking calculation employing the specific combination of influential factors was quantitatively expressed as the rmsd of the docked orientation and the crystallographically determined orientation (Table 3).

DISCUSSION

X-ray analyses of LinB complexed with 1,2-DCE and 1,2-DCP show that these compounds bind nonproductively in the active site of the enzyme, while for 1-CB, the reaction

Table 3: Root-Mean-Square Deviations (Å) between Crystal and Docked Ligand Orientations^a

	complexes		substrates				product	
	halogen anion	active site waters	1,2-DCE		1,2-DCP		1-butanol	
			molecule I	molecule J	molecule I	molecule J	molecule I	molecule J
model 1	–	–	4.4	4.7	4.5	4.1	NA ^b	NA ^b
model 2	+	–	3.6	3.7	3.6	3.8	4.2	4.0
model 3	+	+	2.7	2.4	1.4	1.8	2.5	2.3
model 4	–	+	2.9	2.5	1.2	1.7	NA ^b	NA ^b

^a Molecule I and molecule J refer to the two ligand molecules in the crystal structures. ^b Not applicable.

products are observed. These observations are in agreement with previous kinetic analyses (4). The data from highly sensitive GC–MS analysis, however, indicate very weak activity of LinB with 1,2-DCE and 1,2-DCP, the values of which are 5500 and 2500 times lower than 1-CB dechlorination activity, respectively. The presence of Cl[–] in the halide binding site in the crystallographically determined 1,2-DCP and 1,2-DCE complexes may derive from the weak activity of LinB toward these substrates or may be a residue from protein purification buffers (which contained Cl[–] ions).

With the exception of residue Asp147, there is little movement of active site residues when comparing the complexes of LinB with the structure of the free enzyme. Slight movements were detected in Asp147; however, Asp147 is not close to the catalytic triad, and it would appear unlikely that this residue assists in the formation of a productive enzyme–substrate complex.

Inhibition kinetics confirm that both 1,2-DCE and 1,2-DCP compete for the active site with 1-CB. The kinetic data for both 1,2-DCE and 1,2-DCP inhibition of 1-CB turnover can be explained by a scheme in which either inhibitor or substrate binds to the active site. The substrate and inhibitors do not bind strictly to the same binding position (Figure 4b); however, the binding positions for inhibitors and substrate overlap.

The docking calculations help explain the nonproductive binding of DCE and DCP in the active site of LinB. Docking should reveal the most energetically favorable binding sites within the active site. In the absence of a water molecule and halide in the docking calculations, the molecules bind productively in terms of both its position and conformation (Figures 2b and 3b). No alternative binding modes were found in these docking calculations. Yet as water and the halide ion are added to the calculation, the ligands adopt orientations increasingly similar to the crystallographically determined positions (Table 3 and Figures 2c and 3c). This result indicates that it is the relative inability of 1,2-DCE and 1,2-DCP to displace active site waters and halide ions compared to the ability of 1-CB that determines their low rate of turnover. Two water molecules in particular appear to be important. These can be seen in Figures 2a and 3a, and are located adjacent to the halide ions observed in these structures. These water molecules appear to form a barrier between 1,2-DCE, 1,2-DCP, and the halide binding site. The water molecules are 3.3 and 3.0 Å from the halide ion and 2.9 and 3.0 Å from the carboxylate oxygen atoms of Asp108, respectively. These stabilizing interactions must be overcome if the ligand is to displace water molecules and bind productively. Interestingly, only one of these water molecules is seen in the complex with 1-butanol (Figure 4a). This water

molecule is also observed in the apoenzyme structure (6).

Notably, small chlorinated substrates (1,1-dichloromethane, 1,2-DCE, and 1-chloropropane) exhibited outlying behavior in the quantitative structure–biodegradability relationship model constructed for 27 substrates of the haloalkane dehalogenase DhaA (26). These substrates exhibited unexpectedly low activity, which could not be directly related to any intrinsic property of these molecules, such as their reactivity, structural, or physicochemical properties. It was proposed that these molecules cannot adopt the proper orientation in the enzyme active site (26). The data presented here agree with this proposal.

The production of enzymes with high activity toward 1,2-DCE and 1,2-DCP is desirable. Mutations in the cap domain of LinB could be introduced to make the nonproductive binding site observed for 1,2-DCE and 1,2-DCP less energetically favorable. Specifically, the mutation of Phe143, Phe151, Val173, Leu177, and Phe169 (all in the cap domain) to bulkier amino acids could have this effect without disrupting the catalytic triad or occluding the active site. These five amino acids form part of the binding pockets for 1,2-DCE and 1,2-DCP and line the active site cavity.

Comparisons with Other Dehalogenases. The catalytic activity of LinB contrasts with that of Dh1A. While 1,2-DCE is an extremely poor substrate for LinB, it is a much better substrate for Dh1A. Direct comparisons between LinB and Dh1A (8) are difficult because the cap domains of the two proteins are very different (27). One consequence of this difference is that the active site of Dh1A dehalogenase (112 Å³) is much smaller than that of LinB (276 Å³). The small size of the Dh1A active site appears only to allow productive binding of 1,2-DCE. LinB, with its relatively large active site, does not restrict 1,2-DCE to bind productively, and appears to provide pockets for the nonproductive binding of 1,2-DCE and other small halocarbons.

The active site of LinB is similar to the *Rhodococcus* dehalogenase DhaA (28), which has an active site cavity only slightly smaller (246 Å³) than that of LinB. Importantly, the residues of the catalytic triad are the same in the two, and many of the hydrophobic residues lining the cavity are conserved (27). Activity of DhaA to 1,2-DCE has not been detected (29), and therefore, a mechanism of water-mediated inhibition observed in LinB could act in DhaA. Further experiments are required to confirm this proposal. Two substitutions that occur in the active site of DhaA are Trp152 and Cys187 (corresponding to Phe143 and Leu177, respectively, in LinB). The existence of these substitutions supports the proposal that mutations of residues in the cap domain of LinB can be created that retain catalytic activity.

CONCLUSIONS

This study shows that the industrially important molecules 1,2-DCE and 1,2-DCP can bind nonproductively in the active site of LinB, and that the low activity of LinB for these substrates appears to result from their inability to displace water and halide molecules from the active site. The water- and product-mediated effects observed in this study could be important for other dehalogenases such as DhaA, which has an active site very similar to that of LinB. The activity of LinB toward small halocarbons such as 1,2-DCE could be improved through the introduction of mutations in the cap domain of the protein that make nonproductive binding less favorable.

ACKNOWLEDGMENT

Dr. Igor Kucera (Biochemistry Department, Masaryk University) is gratefully acknowledged for valuable advice on the presentation of enzyme kinetics data and Jana Sykorova (National Centre for Biomolecular Research, Masaryk University) for technical assistance with protein purification.

REFERENCES

- Copley, S. D. (1998) *Curr. Opin. Chem. Biol.* 2, 613–617.
- Fetzner, S., and Lingens, F. (1994) *Microbiol. Rev.* 58, 641–685.
- Fetzner, S. (1998) *Appl. Microbiol. Biotechnol.* 50, 633–657.
- Nagata, Y., Miyauchi, K., Damborsky, J., Manova, K., Ansorgova, A., and Takagi, M. (1997) *Appl. Environ. Microbiol.* 63, 3707–3710.
- Nagata, Y., Nariya, T., Ohtomo, R., Fukuda, M., Yano, K., and Takagi, M. (1993) *J. Bacteriol.* 175, 6403–6410.
- Marek, J., Vevodova, J., Smatanova, I., Nagata, Y., Svensson, L. A., Newman, J., Takagi, M., and Damborsky, J. (2000) *Biochemistry* 39, 14082–14086.
- Ollis, D. L., Cheah, E., Cygler, M., Dijkstra, B., Frolov, F., Franken, S. M., Harel, M., Remington, S. J., Silman, I., and Schrag, J. (1992) *Protein Eng.* 5, 197–211.
- Verschuere, K. H., Seljee, F., Rozeboom, H. J., Kalk, K. H., and Dijkstra, B. W. (1993) *Nature* 363, 693–698.
- Hynkova, K., Nagata, Y., Takagi, M., and Damborsky, J. (1999) *FEBS Lett.* 446, 177–181.
- Anonymous (1993) *Chem. Eng. News* 71, 38–46.
- von Wintzingerode, F., Schlötelburg, C., Hauck, R., Hege-
mann, W., and Gobel, U. B. (2001) *FEMS Microbiol. Ecol.* 35, 189–196.
- Pries, F., van der Ploeg, J. R., Dolting, J., and Janssen, D. B. (1994) *FEMS Microbiol. Rev.* 15, 279–295.
- Smatanova, I., Nagata, Y., Svensson, L. A., Takagi, M., and Marek, J. (1999) *Acta Crystallogr. D55*, 1231–1233.
- Otwinowski, Z., and Minor, W. (1997) in *Methods in Enzymology. Volume 276: Macromolecular Crystallography, part A*, pp 307–326, Academic Press, New York.
- Brunger, A. T., Adams, P. D., Clore, G. M., DeLano, W. L., Gros, P., Grosse-Kunstleve, R. W., Jiang, J. S., Kuszewski, J., Nilges, M., Pannu, N. S., Read, R. J., Rice, L. M., Simonson, T., and Warren, G. L. (1998) *Acta Crystallogr. D54*, 905–921.
- Perrakis, A., Morris, R. J., and Lamzin, V. S. (1999) *Nat. Struct. Biol.* 6, 458–463.
- Jones, T. A., Zou, J. Y., Cowan, S. W., and Kjeldgaard, M. (1991) *Acta Crystallogr. A47*, 110–119.
- Kleywegt, G. J., and Jones, T. A. (1998) *Acta Crystallogr. D54*, 1119–1131.
- Collaborative Computational Project, No. 4 (1994) *Acta Crystallogr. D50*, 760–763.
- Kleywegt, G. J. (1997) *J. Mol. Biol.* 273, 371–376.
- Kleywegt, G. J. (1996) *Acta Crystallogr. D52*, 842–857.
- Goodsell, D. S., and Olson, A. J. (1990) *Proteins* 8, 195–202.
- Vriend, G. (1990) *J. Mol. Graphics* 8, 52–56.
- Morris, G. M., Goodsell, D. S., Halliday, R. S., Huey, R., Hart, W. E., Belew, R. K., and Olson, A. J. (1998) *J. Comput. Chem.* 19, 1639–1662.
- Solis, F. J., and Wets, R. J. B. (1981) *Math. Oper. Res.* 6, 19–30.
- Damborsky, J., Manova, K., and Kutý, M. (1996) in *Biodegradability Prediction*, pp 75–92, Kluwer Academic Publishers, Dordrecht, The Netherlands.
- Damborsky, J., and Koca, J. (1999) *Protein Eng.* 12, 989–998.
- Newman, J., Peat, T. S., Richard, R., Kan, L., Swanson, P. E., Affholter, J. A., Holmes, I. H., Schindler, J. F., Unkefer, C. J., and Terwilliger, T. C. (1999) *Biochemistry* 38, 16105–16114.
- Schindler, J. F., Naranjo, P. A., Honaberger, D. A., Chang, C.-H., Brainard, J. R., Vanderberg, L. A., and Unkefer, C. J. (1999) *Biochemistry* 38, 5772–5778.

BI015734I